

## **A three-dimensional model of wave attenuation in the marginal ice zone**

**Luke G. Bennetts, Malte A. Peter, V. A. Squire, Michael H. Meylan**

### **Angaben zur Veröffentlichung / Publication details:**

Bennetts, Luke G., Malte A. Peter, V. A. Squire, and Michael H. Meylan. 2010. "A three-dimensional model of wave attenuation in the marginal ice zone." *Journal of Geophysical Research* 115 (C12): C12043. <https://doi.org/10.1029/2009JC005982>.

### **Nutzungsbedingungen / Terms of use:**

**licgercopyright**

Dieses Dokument wird unter folgenden Bedingungen zur Verfügung gestellt: / This document is made available under the following conditions:

**Deutsches Urheberrecht**

Weitere Informationen finden Sie unter: / For more information see:

<https://www.uni-augsburg.de/de/organisation/bibliothek/publizieren-zitieren-archivieren/publizieren>



## A three-dimensional model of wave attenuation in the marginal ice zone

L. G. Bennetts,<sup>1</sup> M. A. Peter,<sup>2</sup> V. A. Squire,<sup>1</sup> and M. H. Meylan<sup>3</sup>

Received 10 November 2009; revised 3 May 2010; accepted 10 September 2010; published 17 December 2010.

[1] A three-dimensional model of wave scattering by a large array of floating thin elastic plates is used to predict the rate of ocean wave attenuation in the marginal ice zone in terms of the properties of the ice cover and the incoming wavefield. This is regarded as a small step toward assimilating interactions of ocean waves with areas of sea ice into oceanic general circulation models. Numerical results confirm previous findings that attenuation is predominantly affected by wave period and by the average thickness of the ice cover. It is found that the shape and distribution of the floes and the inclusion of an Archimedean draft has little impact on the attenuation produced. The model demonstrates a linear relationship between ice cover concentration and attenuation. An additional study is conducted into the directional evolution of the wavefield, where collimation and spreading can both occur, depending on the physical circumstances. Finally, the attenuation predicted by the new three-dimensional model is compared with an existing two-dimensional model and with two sets of experimental data, with the latter producing convincing agreement.

**Citation:** Bennetts, L. G., M. A. Peter, V. A. Squire, and M. H. Meylan (2010), A three-dimensional model of wave attenuation in the marginal ice zone, *J. Geophys. Res.*, *115*, C12043, doi:10.1029/2009JC005982.

### 1. Introduction

[2] Immense regions of sea ice encircle the Antarctic continent, stretching far into the Southern Ocean and seasonally expanding and contracting the cryosphere. The existence of this natural barrier is fundamental to the survival of the ice shelves and ice tongues that abound along the continent's coastline [Squire *et al.*, 1994; Cathles *et al.*, 2009]. But sea ice is also an immensely geophysically significant substance itself, which, for example, influences marine ecology and affects the global climate system. The latter contribution is largely due to the summer ice albedo feedback mechanism [Hall, 2004], but other factors, such as the production of dense water during freezing and the expulsion of fresh water during melting are also important [Feltham, 2008].

[3] The ocean wave motion that most affects sea ice, the topic of this work, is confined to a dynamic region known as the marginal ice zone (MIZ) that reaches for tens to hundreds of kilometers from the ice margin into the ice pack [Squire *et al.*, 1995]. Thereabout the ocean surface is a mixture of sea ice and open water, where the ice consists of many different floes of varying shapes and sizes that are free to move

their position within the mélange when acted upon by winds and waves.

[4] The proportion of a wave that withstands reflection at the ice edge and is transmitted into the pack causes the ice floes to flex. In doing so, a strain is imposed on the ice that may weaken it and, if large enough, cause fracture and subsequent breakup [Langhorne *et al.*, 2001]. As the wave progresses deeper into the ice pack, it is attenuated through diffraction that arises as it meets each floe in its path, and additionally by other natural agents such as hysteresis in the sea ice and collisions between nearby floes [Squire *et al.*, 1995]. An intimate relationship between the configuration of the ice cover in the MIZ and the traveling waves arises whereby the ice cover removes energy from the waves while the waves determine the morphology of the ice cover. Evidence of this is seen in the formation of floes into zones of increasing diameter ordered in distance away from the ice edge [Squire and Moore, 1980].

[5] Although rising temperatures are believed to be the primary threat to sea ice, it is conjectured that its effect is compounded by ocean waves. Direct wave-induced melting has been confirmed as significant by Wadhams *et al.* [1979], especially in the outer regions of the MIZ. However, penetrating ocean waves also act to break up floes, allowing increased contact between local open water and ice, which hastens the annihilation of sea ice indirectly under summer conditions at least. Disturbing the balance between waves and sea ice with a reduction in the strength, compaction, and extent of the ice cover leads to increased wave activity and a corresponding amplification of these direct and indirect destructive agents, thus defining a positive feedback loop. In addition to these climatological implications, the presence of

<sup>1</sup>Department of Mathematics and Statistics, University of Otago, Dunedin, Otago, New Zealand.

<sup>2</sup>Institute of Mathematics, University of Augsburg, Augsburg, Germany.

<sup>3</sup>Department of Mathematics, University of Auckland, Auckland, New Zealand.

waves in regions of sea ice is a consideration for the engineering activities that take place in its vicinity.

[6] While sea ice has been integrated into many contemporary global climate models, at present there exists no mechanism for assimilating the influence of ocean waves on the sea ice. The purpose of the work presented herein is to study the evolution of long-crested ocean waves of a prescribed period through the MIZ, given a snapshot of the prevailing ice conditions. In this sense, it can be regarded as a small step toward providing a coupled waves and sea ice component for use in an oceanic general circulation model.

[7] The ability to describe the propagation of waves that travel through regions of ice-covered fluid has received a considerable amount of attention in the past 20 years. From the highly idealized early models, the science has now advanced to the stage at which properties such as ice of varying thickness and a correct Archimedean draft can be accommodated [Bennetts *et al.*, 2007, 2009] and the consideration of scattering by three-dimensional floes of arbitrary shape is possible [Meylan, 2002]. A summary of the recent advances in the theory of waves and sea ice is presented by Squire [2007]. However, assumptions of linear motions and harmonic time dependence remain a feature among these works, and the concept of treating the sea ice as a thin elastic plate is universal.

[8] The next step is to reconstruct a region of sea ice of realistic proportions by combining a large number of scattering sources, and this presents its own significant challenges. Dixon and Squire [2001] attempted this using a coherent potential approximation. However, the investigation was confined to two dimensions, and a three-dimensional extension is thus far lacking.

[9] Efforts to model wave propagation in the MIZ have also been made in the past by simplifying interactions so that they are in terms of energy alone. The first attempt of this kind was made by Wadhams [1986] for a two-dimensional geometry. This was extended to three dimensions by Masson and LeBlond [1989], and nonlinear wave coupling, dissipation of wave energy, and wind-wave generation were accounted for, notwithstanding the assumption of isotropy of the ice cover to generate numerical solutions. In an ensuing work, Perrie and Hue [1996] combined the approach of Masson and LeBlond [1989] with an operational wave model to predict wave attenuation in the MIZ. However, although they included three degrees of motion and draft, both of these works were restricted by the need to model the floes as rigid circular bodies. Flexure of the ice was accommodated by Meylan *et al.* [1997] in a zero-draft floe model based on a linear Boltzmann (or transport) equation, which has recently been shown by Meylan and Masson [2006] to be almost identical to the multiple scattering theory of Masson and LeBlond [1989].

[10] In the energy scattering descriptions developed in the above papers, wave interactions take place without the consideration of phase effects. However, evidence now suggests that the accurate calculation of average attenuation is highly dependent on the inclusion of such features [Berry and Klein, 1997]. Although relevant theories exist for interactions that acknowledge the phase of waves [e.g., Peter and Meylan, 2004], in practice a direct application to an ice covering on the scale we wish to investigate is a massive and fanciful numerical undertaking. For this reason, previous investiga-

tions, notably Kohout and Meylan [2008], Vaughan *et al.* [2009], and Squire *et al.* [2009], have been restricted to homogeneity in one horizontal dimension. While the latter two studies were primarily concerned with wave evolution in the Arctic Basin, where the sea ice forms a quasi-continuous veneer, the MIZ is composed of many separate floes and it is widely accepted that to represent it faithfully demands a fully three-dimensional theory. In this sense, the current work can be viewed as an extension of Kohout and Meylan [2008].

[11] Recently, two similar but independent mathematical methods have been developed by the authors for modeling wave scattering in the MIZ [Bennetts and Squire, 2009a, 2009b; Peter and Meylan, 2009a, 2009b]. These models treat the MIZ as a three-dimensional expanse assembled from a vast collection of floes that are simultaneously individual and interrelated. In the models, the MIZ is idealized as an array that is fashioned from a large number of rows, where each row consists of an infinite number of floes and it is possible to vary the properties of the floes and the various spacings involved. To combine the motions of the floes in a row, a periodicity condition is applied, and a common periodicity is required of the array as a whole to harmonize the row interactions.

[12] In the current work, we combine the two methods and fulfill the role that the underlying model was originally conceived to replicate as a basis for investigating the attenuation of long-crested ocean waves in the MIZ due to diffraction by floes. The availability of two different methods that agree so well, for such a complicated situation, gives us great confidence in our output, but their relative strengths also complement one another and allow us to examine how characteristics of the MIZ, such as floe shape and concentration, determine the degree of attenuation produced.

[13] The following section begins by outlining the three-dimensional mathematical model of the MIZ and giving a brief overview of the two solution methods. At the end of section 2, the process of extracting an attenuation coefficient, and in particular the use of ensemble averaging to eliminate obstructive coherence effects, is discussed. Subsequently, in section 3, we conduct a numerical investigation into the dependence of the attenuation coefficient on several key properties of the MIZ, focusing on those that are new to our model, such as concentration, draft, floe shape, and directionality. The section finishes by contrasting the attenuation predicted by our three-dimensional model with that of the two-dimensional model of Kohout and Meylan [2008]. In section 4, two sets of experimental data on wave attenuation in the MIZ are chosen for comparison with our model and a generally creditable agreement is found. To conclude, a summary of the work presented in this article is given in section 5.

## 2. The Three-Dimensional Mathematical Model

### 2.1. Preliminaries

[14] We visualize the MIZ as an array consisting of a large number of sea-ice floes floating on an otherwise open fluid domain of finite depth  $h$  that is infinite in all horizontal directions. The principal attribute of the physical situation we wish to investigate is the attenuation of ocean waves due to the scattering produced by the floes. We therefore disregard processes such as viscosity and floe collisions. The region of

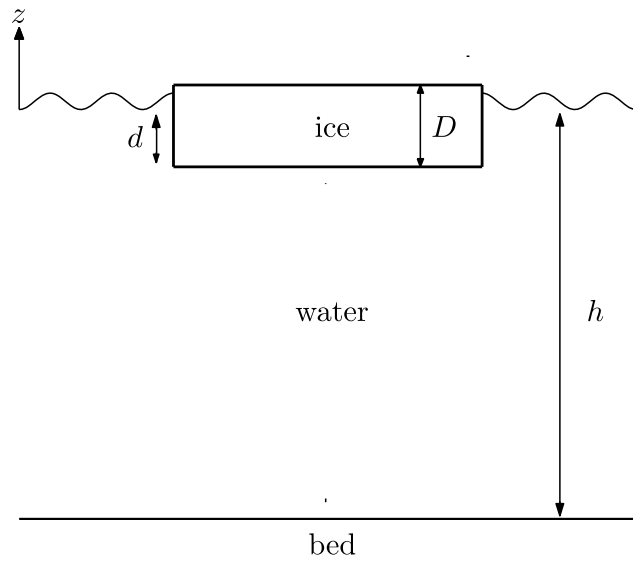


**Figure 1.** The geometry in the vertical plane including a typical floe.

the horizontal plane occupied by the ice cover is considered fixed, and the surge response of the floes is neglected.

[15] The array is composed of a series of rows, in which each row contains an infinite number of modules of floes with some prescribed periodicity imposed to facilitate a solution. For the majority of our investigation, the modules contain a single floe only, so that the rows consist of identical floes. However, in section 3.3, the effects of including an additional floe in the modules, which allows for a nonuniform distribution of floes in the rows, is studied. The dimensions of the ice cover are assumed to be known but are randomized to simulate the natural heterogeneity of the situation. Its structural properties are also considered known, with its flexural rigidity given by  $F = YD^3/12(1 - \nu^2)$ , where we set the Young’s modulus for sea ice as  $Y = 6 \times 10^9$  Pa and Poisson’s ratio as  $\nu = 0.3$ , these being typical values, and  $D$  denotes the ice thickness. Each floe in the array is free to flex indepen-

dently of its neighbors, but its motion is affected by the waves diffracted away from all of the other floes. The geometry just described is depicted in Figures 1 and 2.

[16] In keeping with other similar studies, we suppose that the waves passing through the MIZ are of small amplitude, so that linear theory may be applied, and we consider solutions at a given period  $\tau$  s. Under these conditions, and assuming an irrotational velocity field, the motion of the fluid may be described using a velocity potential  $\Phi = \Phi(x, y, z)$ . The coordinates  $x$  and  $y$  determine the position in the horizontal plane, with  $y$  oriented so that it lies parallel to the rows and  $z$  is the vertical coordinate that points directly upward and has its origin set to coincide with the fluid surface in the absence of ice (see Figure 1). Treating the fluid as incompressible and inviscid, the velocity potential,  $\Phi$ , is governed throughout the fluid domain by Laplace’s equation,

$$\nabla^2 \Phi = 0 \quad (x, y \in \mathbb{R}^2),$$

for  $-h < z < 0$  when ice does not occupy the fluid surface and for  $-h < z < -d$  when ice is present, where  $d = (\rho_i/\rho_w)D$  is the draft of the floes, in which  $\rho_i = 922.5 \text{ kg m}^{-3}$  is the density of sea ice and  $\rho_w = 1025 \text{ kg m}^{-3}$  is the density of the underlying water. On the ocean bed,  $z = -h$ , the no-flow condition  $\Phi_z = 0$  holds, and on the linearized fluid surface away from the floes,  $z = 0$ , we have the free-surface condition  $\Phi_z = \sigma\Phi$ , where the frequency parameter is  $\sigma = (1/g)(2\pi/\tau)^2$  and  $g \approx 9.81 \text{ m s}^{-2}$  is acceleration due to gravity.

[17] Sea ice forms floes that have horizontal dimensions that far exceed their thicknesses, so that fluid motion will induce a flexural response [Squire *et al.*, 1995]. Combined with the assumption of small-amplitude waves, this fact motivates the modeling of sea ice as a thin elastic plate, for which points in a vertical plane retain their alignment under deformation [Timoshenko and Woinowsky-Krieger, 1959]. For a thin elastic plate, it is possible to calculate the stresses and strains experienced by the ice under fluid motion from knowledge of the displacement it undergoes on its lower surface, denoted  $W = W(x, y)$ .

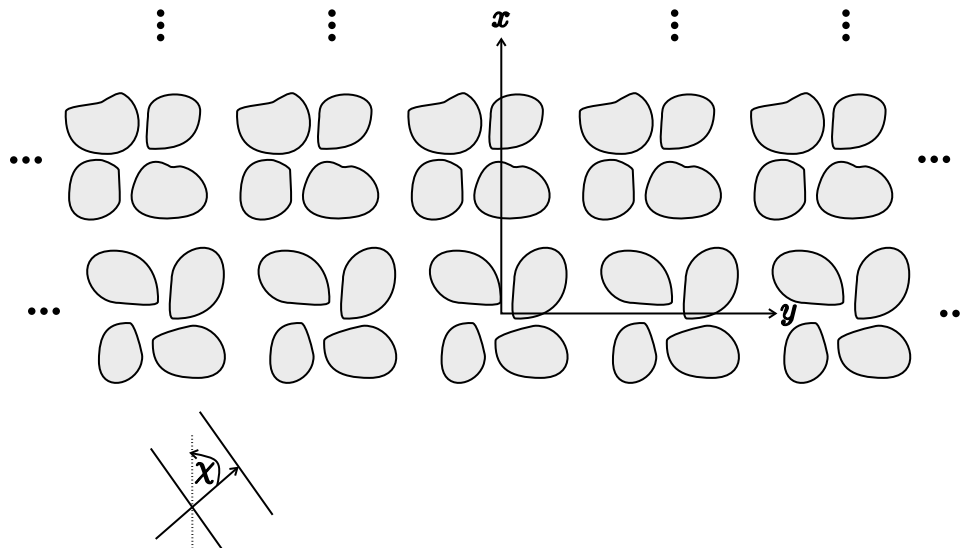


**Figure 2.** The geometry in the horizontal plane. In this case, the modules contain four floes.

[18] At the fluid-ice interface, the velocity potential and displacement function are linked by relating the thin elastic plate equation, which describes the motion of the ice in terms of the difference in pressure at its lower surface and the (constant) atmospheric pressure, to the linearized version of Bernoulli's equation, which provides an expression for the fluid pressure beneath the ice. This assumes no cavitation between the ice and the fluid. Adding a linearized kinematic condition to these equations results in the coupling

$$(1 - \sigma d)W + (F/\rho_w g)(W_{xx} + W_{yy})^2 - \Phi = 0,$$

which is applied at the linearized fluid-ice interface  $z = -d$ . There are also so-called free-edge conditions, which impose the vanishing of the ice's bending moment and shearing stress and must be enforced at the perimeter of each floe. These are represented through the equations

$$W_{xx} + W_{yy} - (1 - \nu)(W_{ss} + \Theta W_n) = 0, \quad (1a)$$

and

$$(W_{xx} + W_{yy})_n + (1 - \nu)W_{sns} = 0, \quad (1b)$$

respectively, and are the natural conditions that occur when Hamilton's principle is applied to the thin elastic plate equations [Porter and Porter, 2004]. In equations (1a) and (1b), the subscript  $n$  denotes differentiation with respect to the normal direction and  $s$  the tangential direction when traversing the perimeter of a floe. The quantity  $\Theta$  denotes curvature. One final condition must hold at the edges of the floes, which describes the fluid's inability to penetrate through the submerged portion of the floe, and is

$$\Phi_n = 0 \quad (-d < z < 0).$$

[19] A long-crested ocean wave,  $\Phi_I$ , is incident on the array of floes and travels from the far-field  $x \rightarrow -\infty$  at an oblique angle  $\chi$  with respect to the  $x$ -axis. This incident wave may be expressed as follows:

$$\Phi_I(x, y, z) = e^{ik(v_0 x + u_0 y)} \cosh\{k(z + h)\},$$

where  $v_0 = \cos \chi$ ,  $u_0 = \sin \chi$  and  $k$  is the propagating wave number, which is defined as the real positive root of the dispersion relation

$$k \tanh(kh) = \sigma.$$

During the scattering process, the array of floes redistributes the energy carried by this wave over a finite number of angles  $\chi_m$  ( $m \in \mathcal{M} \subset \mathbb{Z}$ ), so that the transmitted wavefield has the form

$$\Phi(x, y, z) \sim \sum_{m \in \mathcal{M}} T_m e^{ik(v_m x + u_m y)} \cosh\{k(z + h)\} \quad \text{as } x \rightarrow \infty, \quad (2)$$

where  $v_m = \cos \chi_m$ ,  $u_m = \sin \chi_m$ , and the  $T_m$  are amplitudes that must be calculated [Peter et al., 2006; Bennetts and Squire, 2009a]. The size of the set of transmitted wave angles varies according to a number of parameters. Typically, in the simulations we are interested in, it consists of only a handful of values ( $\leq 5$ ) and often merely the incident wave

angle. An investigation of the directional spectrum is made in section 3.1.

[20] To produce the results for our investigation, two solution methods for the geometrical situation described above are utilized. Possessing two such solution methods, which have been formulated independently and employ different mathematical techniques, has allowed us to validate thoroughly the results that we present. Moreover, although the two methods solve essentially the same problem, each one has its own particular advantages that allow us to probe certain features of the ice cover.

[21] Details of these methods are described by Bennetts and Squire [2009a, 2009b] and Peter and Meylan [2009a, 2009b], respectively. These previous works formulated the solution procedures and investigated the main mathematical and computational properties contained therein. In contrast, the current work focuses on the physical implications that can be drawn from using this three-dimensional model. To achieve this, we make use of the key findings presented by Bennetts and Squire [2009a, 2009b] and Peter and Meylan [2009a, 2009b], which are outlined in the following two subsections.

## 2.2. Row Spacing

[22] Between the rows of ice floes, both propagating and evanescent waves exist. However, for numerical expediency, in the current work, it is assumed that the interactions consist only of the former, with the latter considered negligible during the process. Such a restriction is well established in many areas of wave interactions, for instance, hydrodynamic problems [see Linton and McIver, 2001] and electromagnetic scattering [e.g., McPhedran et al., 1999], and in the former it is often termed a wide-spacing approximation (WSA). Although it is possible to incorporate the effects of the evanescent waves in the interactions, it was shown by both Bennetts and Squire [2009b] and Peter and Meylan [2009a] that the restriction to propagating waves only is of high accuracy and numerically efficient.

[23] Moreover, it has been mentioned already that our model only accounts for attenuation caused by scattering, with waves propagating unhindered through open water. Thus the use of the WSA makes it explicit that the spacing between rows will only affect the phase of the waves traveling between them. Any resulting modulation of the transmitted energy will be eradicated by sufficient averaging, and thus row spacing ceases to be a determinant of the attenuation properties. This has no implications for our attenuation coefficient,  $\alpha$ , which is defined in the following section, owing to the nondimensionalization employed but it has important ramifications for the concept of concentration that is discussed in section 3.4.

## 2.3. Attenuation

[24] It is well established through experimental evidence [e.g., Wadhams, 1975, 1978; Squire and Moore, 1980] that wave energy attenuates exponentially through the MIZ and that this attenuation acts as a low-pass filter that favors the transmission of long waves. Exponential attenuation is also a property of linear models such as the one employed in this work [Kohout and Meylan, 2008]. Our investigation centers on the degree of attenuation arising from certain key attributes of the ice cover, such as its concentration on the ocean surface and ice thickness.

[25] To study wave attenuation, we define the transmitted energy  $E$  to be

$$E = \frac{1}{v_0} \sum_{m \in \mathcal{M}} |T_m|^2 v_m,$$

which is the wave energy traveling in the direction of the incident wavefield taken over the discrete spectrum of angles generated by the array of floes. The value of this quantity will depend on both the properties of the incident wavefield and the ice cover, in particular the number of rows,  $\Lambda$  say, comprising the array. As described above, we expect  $E$  to decay exponentially with distance through the MIZ, and thus, following *Kohout and Meylan* [2008], we may separate the dependence of the transmitted energy on row number by writing

$$E = e^{-\alpha\Lambda}, \quad (3)$$

where  $\alpha$  is referred to as the (nondimensional) attenuation coefficient.

[26] The primary objective of this work is to determine the behavior of the attenuation coefficient, as parameters such as ice thickness and wave period are varied, and also to compare these results to those already existing for simplified two-dimensional models of the MIZ and experimental data. This requires us to extract an attenuation coefficient from our three-dimensional model. The process that is required to achieve this is complicated by the occurrence of constructive and destructive coherence. For instance, waves may resonate over the length of a row and a row separation if this scale occurs too many times (so-called Bragg resonance) [see *Bennetts and Squire*, 2009b], and this will produce an artificially large attenuation over a wide range of periods. It is also possible for resonances emanating from individual rows to contaminate results unless care is taken in the calculation of the attenuation coefficient.

[27] An established method to avoid these inhibiting resonance effects is to perform ensemble averaging [see *Kohout and Meylan*, 2008]. Specifically, we construct  $E$  as a function of  $\Lambda$  by taking the mean of the transmitted energies given by a large number of arrays, typically 100, in which certain key parameters are distributed normally around given values. The exponential decay, described in equation (3), of this averaged function is then calculated using a least squares approach to yield the attenuation coefficient  $\alpha$ . In the Results section, the particular methods of averaging used are described in detail along with their relation to the type of resonance that necessitates their implementation.

### 3. Simulation of Attenuation in the MIZ

[28] In this section, the relative influence of the various parameters that exist in the problem on the rate of attenuation is investigated. In doing so, we wish to extend the study of *Kohout and Meylan* [2008]. Using a two-dimensional model of the MIZ, *Kohout and Meylan* [2008] found that the rate of attenuation is primarily determined by ice thickness and wave period. Clearly, thickness and period will also be important parameters in our model. However, in our three-dimensional model, there are many additional features that may be of

importance to the passage of waves through an ice-covered ocean that can be investigated.

#### 3.1. Directionality

[29] We begin by investigating the effect of the angle of the incident wave on attenuation. Recall that in our model it is possible to set the direction at which the crest of the incident wave affects the array by means of the parameter  $v_0 = \cos \chi$ , which ranges from normal incidence  $v_0 = 1$  to grazing incidence  $v_0 = 0$ . This then modifies the angles at which waves travel within the array and are ultimately transmitted (see equation (2)). Note that because we measure attenuation normalized with respect to the incident angle, the change in the distance that must be traveled by waves through the ice pack as  $v_0$  is varied will not be reflected in the value of  $\alpha$ .

[30] Figure 3 displays the attenuation coefficient  $\alpha$  as a function of the cosine of incident angle,  $v_0$ , for three different wave periods  $\tau = 8$  s, 12 s, and 16 s, which correspond to the incident wavelengths of approximately 100 m, 225 m, and 400 m, respectively. The floes that form the array are all circular, of radius 10 m and with an in-row spacing, defined as the distance between the closest points of adjacent floes of 5 m. Draft, which is investigated in the next section, is neglected. In Figures 3a–3c, the results for two ice thicknesses  $D = 0.5$  m and 2 m are given, and a least squares straight-line fit is overlaid on each data set.

[31] Note that the ordinate axes here are on a log scale. It is apparent from these data that there is a nearly exponential dependence of the attenuation coefficient on the incident angle, with normal incidence (at the right-hand end of Figures 3a–3c) experiencing the least attenuation. However, the straight-line fits do not match the data so well as the angle of incidence becomes close to parallel with the array and this feature becomes more pronounced for longer waves. This is due to resonant behavior at grazing incidence when all of the incoming wave is reflected [see *Linton and Thompson*, 2007].

[32] The influence of the incident angle on the attenuation rate is greatest at lower periods. Here we see a difference of more than an order of magnitude between the two ends of the range of angles for the 8 s waves, which decreases to approximately half an order of magnitude for 16 s waves. It is also striking that the ice thickness has negligible influence over the functional behavior of  $\alpha$  with  $v_0$ , with the corresponding curves lying virtually parallel to one another.

[33] To give a more visual appreciation of the way in which the direction of an incident wave is modified as it travels through the MIZ, Figure 4 shows an evolved energy spectrum for the arrays considered in Figure 3 with 2 m ice thickness. In Figure 4, the transmitted energy is given as a function of incident wave angle after 300 rows, which corresponds to approximately a 10 kilometer penetration into ice-covered water. The incoming wave energy is taken as a cosine-squared distribution around normal incidence, and this is also shown.

[34] Even after this distance into the MIZ, the energy transmitted in the 16 s case is barely distinguishable from that of the incident wave. In the 12 s case, the wave energy has experienced attenuation, but despite this, approximately 90% of the central wave packet remains and the qualitative nature of the incident wave is undisturbed. Attenuation of the 8 s wave, however, is far more pronounced. For instance, only around half of the incoming wave energy traveling straight

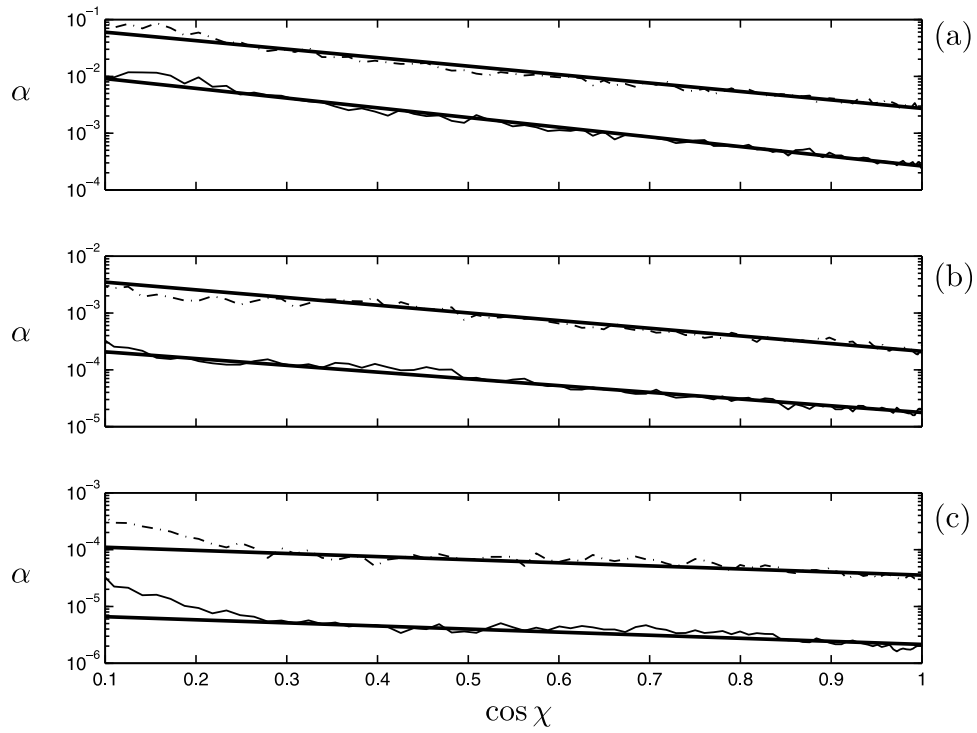


**Figure 3.** The attenuation coefficient against the cosine of the incident angle for an array of circular floes that have a 10 m radius and are 0.5 m thick (solid lines) or 2 m thick (broken lines), with straight-line fits superimposed (thick lines). The in-row spacing is 5 m, and submergence is neglected. (a) 8 s waves. (b) 12 s waves. (c) 16 s waves.

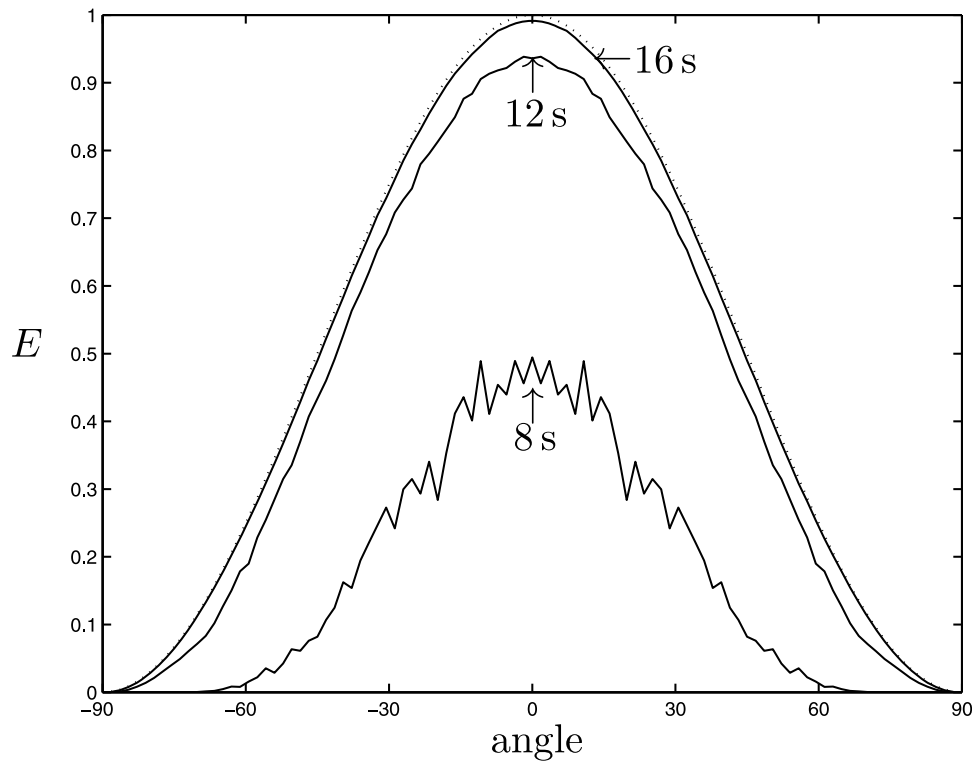


**Figure 4.** The transmitted energy  $E$  as a function of angle after 300 rows. The row geometry is identical to that in Figure 3. Wave periods 8 s, 12 s, and 16 s are shown (solid lines) along with the energy distribution of the incident wavefield (dotted).

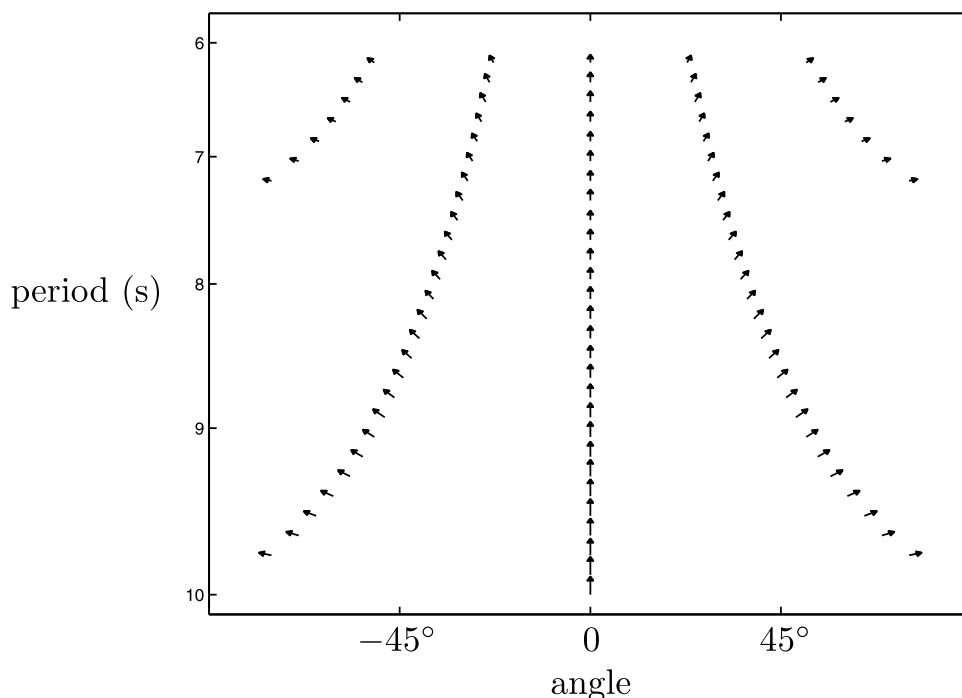


**Figure 5.** Vectors depicting the components of the energy transmitted by an array composed of 100 rows. The floes used in the array have mean thickness 1 m and diameter 100 m, and the in-row separation is 50 m. The direction of the vectors denotes the angle of the transmitted waves, the vertical being normal to the array, and their magnitudes are derived from the value of the energy carried by the particular wave.

through the array still exists. Furthermore, as predicted by the previous figure, the attenuation of the energy increases with incident angle and no discernible energy remains traveling beyond a  $65^\circ$  angle.

[35] From the investigation conducted in this section thus far, we therefore deduce an exponential dependence of the attenuation on the direction of the incident wave, with its rate highly dependent on the wave period. Having established this, unless otherwise stated, for simplicity we proceed using only normal incidence ( $v_0 = 1$ ).

[36] There is another interesting aspect to the question of directionality in our three-dimensional model. It was mentioned earlier that, as well as directly attenuating the amplitude of the incident wave, the array of floes may transmit waves that travel in other directions (cf. equation (2)). However, supplementary waves will only be generated under certain conditions. In particular, large floes and long in-row separations allow more scope for auxiliary waves to be created and, often in simulations where the arrays are tightly packed and consist of relatively small floes, no such waves will be seen. Nevertheless, for a given geometry, if small enough periods are considered, then extra waves are always produced, and for some cases the period range in which this takes place is physically admissible.

[37] In Figure 5, we consider a feasible situation in which multiple waves are transmitted by the array. Here the array is composed of 100 rows of floes of diameter 100 m and mean thickness 1 m, with an in-row separation of 50 m. Through the use of vectors, Figure 5 depicts the cut-in of additional waves as period decreases, as well as the subsequent development of their properties. The direction of the vectors themselves indicates the angles of the waves, and their

magnitudes denote the proportion the corresponding waves contributes to the transmitted energy  $E$ , which is scaled logarithmically.

[38] For the range of periods used in Figure 5, there are two instances of waves cutting in at approximately 8.9 s and 6.2 s. The extra waves occur in pairs, with each of equal magnitude and directionally symmetric about the incident wave angle. It is clear that as waves cut in, they do so at grazing incidence and are only of negligible magnitude. The angles then evolve smoothly, approaching that of the incident wave, and they contribute an increasingly large proportion of the overall traveling wave energy. This quantity is therefore continuous at the points for which the number of propagating waves changes, although, as we will see, it does change rapidly over the surrounding intervals.

[39] Experimental evidence suggests that the directional wavefield broadens within the MIZ [Wadhams *et al.*, 1986]. Moreover, isotropy can be attained close to the ice edge over a distance as short as a kilometer, but this is heavily dependent on the salient wave period, with long periods only displaying such tendencies much farther into the ice pack. The cause of a directional widening has been attributed to lateral scattering effects [Squire *et al.*, 1995], which compete with collimating effects that, in contrast, act to narrow the wave spectrum. The latter can be discerned, although only slightly, in Figure 4.

[40] Owing to the restraints they impose on the geometry, two-dimensional models are only able to simulate collimation, whereas in our three-dimensional model, floes are free to scatter waves in all directions and thus both features are accommodated. While we are careful not to assert that our model exactly replicates the physical phenomenon of wave spreading, it is nonetheless striking that it does account for a

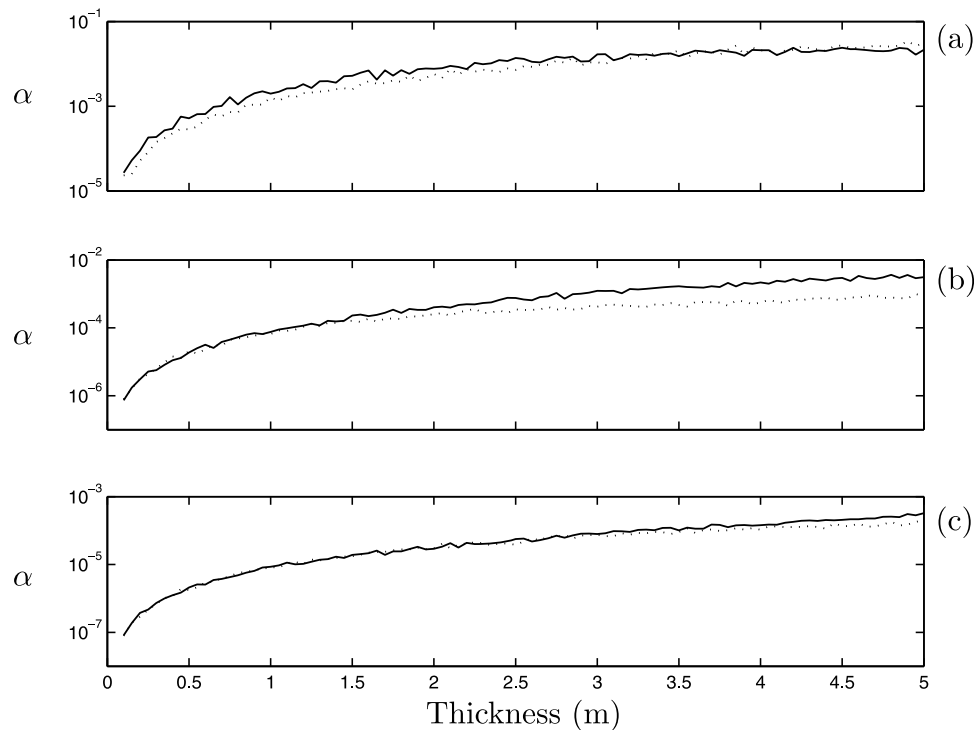


**Figure 6.** The attenuation coefficient  $\alpha$  as a function of mean floe thickness comparing ice cover in which an Archimedean draft is accommodated (solid curves) with ice cover that uses zero draft (broken curves). The three subplots show the periods (a) 8 s, (b) 12 s, and (c) 16 s. The row geometry is identical to that in Figure 3.

widening of the transmitted wavefield at lower periods. However, the discrete manner in which the supplementary waves appear may be somewhat artificial in the context of wave scattering in the MIZ, and we will seek methods to refine this attribute when developing future models.

### 3.2. Draft

[41] We now turn to the effects caused by the introduction of draft into the model so that the floes are neutrally buoyant. This requires that the floes obey the Archimedean principle, and, for the relative values of our chosen ice and water densities, the draft for each floe must therefore be 90% of its thickness, that is,  $d = 0.9D$ .

[42] The addition of draft to a mathematical model of an ice sheet and an ice floe has been studied previously [see *Bennetts et al.*, 2007, 2009; *Williams and Squire*, 2008; *Williams and Porter*, 2009], and it has been shown that it may significantly increase the amount of wave scattering produced, particularly for prominent features such as large pressure ridges, although the effects arising for a floe are more subtle. However, the inclusion of draft in conjunction with flexure in a realistic ice field comprising a vast number of interacting floes has not been conducted previously.

[43] For a range of ice thicknesses, Figure 6 compares the attenuation coefficients produced by arrays in which draft is neglected and arrays in which draft is accommodated. In all other respects, the arrays are identical and they are made up of circular floes of radius 10 m with an in-row separation of 5 m. The three wave periods 8 s, 12 s, and 16 s are shown by Figures 6a–6c. In addition to averaging the distance between the rows, in these results, the ice thickness has also been

varied using a normal distribution around the given mean value to eliminate length resonances.

[44] As would be expected, it is clear that the general trend is for the addition of a physically admissible draft to cause greater attenuation. Moreover, in most cases, this feature is accentuated by thicker ice. However, the relationship between the corresponding Archimedean draft and zero draft curves is not always so simple. In particular, we note that for an 8 s period and mean thicknesses beyond approximately 3.5 m, the array of zero draft floes attenuates an equal amount or slightly more than the corresponding array of Archimedean draft floes. This is a complicated case, though, in which much scattering is produced by both arrays and the influence of the submergence can be perceived to be relatively small.

[45] In the results presented here, the addition of submergence never causes the attenuation coefficient to deviate as much as an order of magnitude from the zero draft model. Those situations in which it does affect the attenuation are for low periods with thin ice and particularly for the midrange period with thick ice, and we note the difference in the corresponding curves for thicknesses up to 2 m for 8 s periods and thicknesses greater than 1.5 m for 12 s periods. These intervals contrast with the results for 16 s periods, for which scattering is minimal so that the introduction of draft is inconsequential and, as a result, the attenuation is only affected marginally.

[46] At this point, we could conclude that it is not essential to include draft in our calculations to predict attenuation accurately. However, the introduction of draft has an important property which is of a computational nature and is not highlighted in Figure 6. It is known for two-dimensional

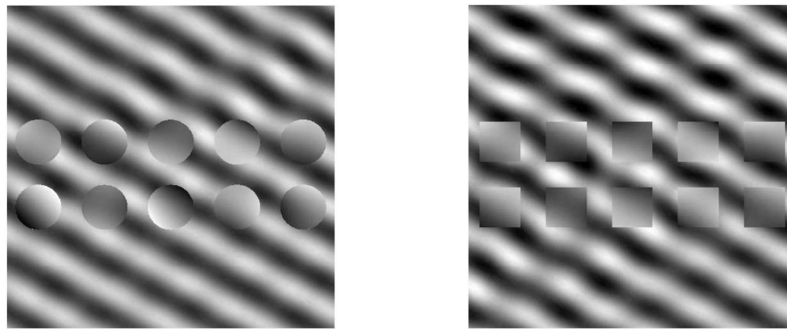


**Figure 7.** Comparison of the scattering caused by (left) circular floes and (right) square floes when used in two-row arrays. Shown are ice-floe displacement and water-surface displacement for an obliquely incident ( $\chi = \pi/6$ ) wave of period 6 s. Although the low wave period distinguishes the relative wavefields, when the number of rows is increased, the resulting attenuation coefficients are very similar (0.0378 for an array of circles and 0.0535 for an array of squares).

models that submergence eliminates the occurrence of perfect transmission [Williams and Porter, 2009] and cannot be attributed to a length scale [Vaughan et al., 2007]. This phenomenon is also true in our three-dimensional model, and numerical tests have shown that the feature is displaced into another regime. An investigation of the causes of this is technical and not aligned with the aim of this paper and will be explored in future work. However, maintaining draft in our model does have the important computational benefit of reducing the extent of averaging that must be performed to calculate an attenuation coefficient that is free of resonances caused by an overly stylized geometry.

### 3.3. Floe Shape and Distribution

[47] Until this point in our investigation, the arrays that we have used have all been composed of circular floes of an identical mean radius. This homogeneity contrasts strongly with the dynamic and heterogeneous nature of the physical phenomenon it is trying to describe. Although we expect that an average property of the array, such as the attenuation it engenders, will be influenced by global properties, such

as concentration (investigated in the following section), no justification for this assumption currently exists. In this section, we therefore investigate the effect of introducing inhomogeneity to the ice cover in the form of noncircular floe shape and a nonuniform distribution of the ice cover.

[48] To demonstrate the influence of floe shape, we compare arrays of square floes and rows of circular floes. For pertinent geometrical parameter sets, it is necessary to use a relatively short incident wavelength for differences to become apparent. An example is given in Figure 7, where we show the wavefields for two rows of alike circles and squares when the wave period is 6 s and the incident angle is  $30^\circ$ . Despite this short wave exposing the particular scattering properties of the floe geometries, when the arrays are extended, the attenuation coefficients produced are very close, with  $\alpha = 0.0378$  for an array of circles and  $\alpha = 0.0535$  for an array of squares. We remark that the wavefields for an 8 s incident wave (not shown) are visually indistinguishable.

[49] In Figure 8, we compare the attenuation caused by arrays of circular and square floes further and simultaneously

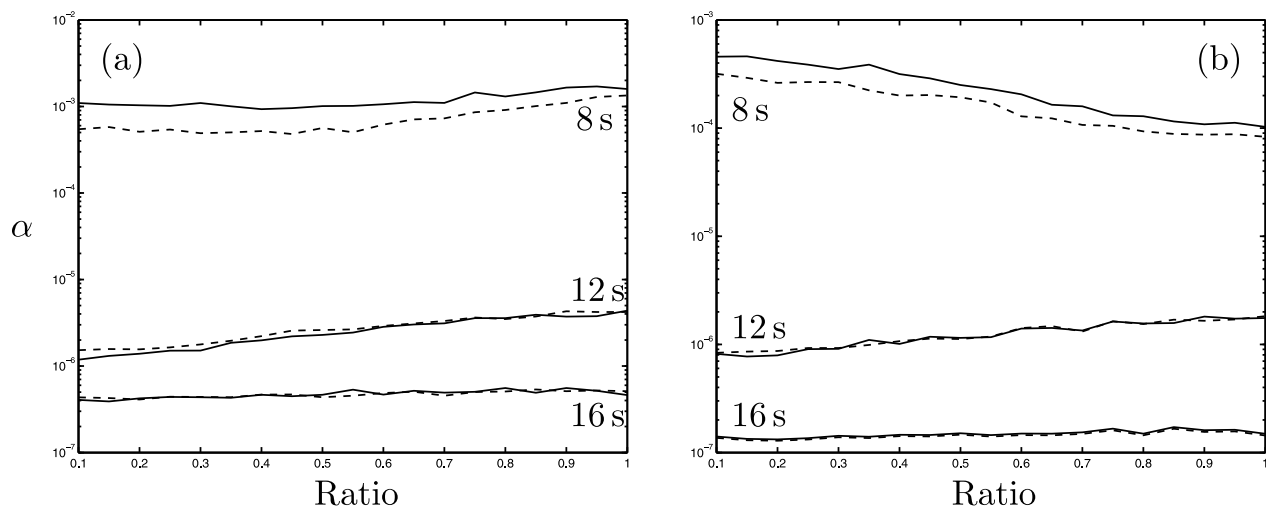


**Figure 8.** The attenuation coefficient as a function of floe-length ratio when the array is composed of modules containing two floes. Results are shown for three different wave periods and for both square floes (solid lines) and circular floes (broken). (a) Higher concentration of larger floes. (b) Lower concentration of smaller floes.

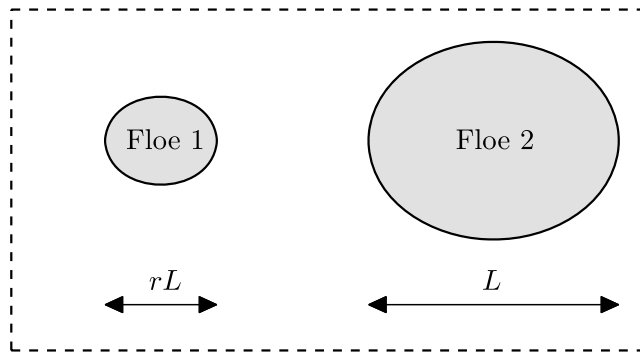


**Figure 9.** An example of a module that is used to obtain the results presented in Figure 8. This particular module contains two circular floes, with the larger one of diameter  $L$  and the smaller one of diameter  $rL$ , where  $r$  is the ratio.

investigate the influence of the distribution of bodies. For this purpose, we consider arrays of modules of two circular or square bodies of different sizes in which the total area covered by ice in each module is constant (a module for the circular case is depicted in Figure 9). The figure shows the attenuation coefficient as a function of the ratio of the length of the two floes, so that unity refers to identical bodies, which is the setting used elsewhere in the paper.

[50] It can be observed that the distance between the corresponding curves produced by arrays of square and circular floes is modest for the lowest wave period considered and decreases as the period becomes larger. Similar behavior occurs when the ice distribution is changed, with attenuation only being affected to a small degree when the wave period is low and less so when the period increases. However, we do note that attenuation by arrays of circular floes is consistently smaller than that of square floes of the same area, which is attributed to less scattering caused by a smoother circular obstacle.

[51] The results presented in this section are representative of the wide range of tests that we have performed. It is therefore concluded that the influence of floe shape and the distribution of the ice cover on attenuation is modest, particularly for longer incident waves. For this reason, our investigation will continue using arrays composed of evenly distributed circular floes, although we recognize that this topic will need further investigation in the future as models become more sophisticated.

### 3.4. Concentration

[52] The influence of the ice pack concentration in determining attenuation is important and, to be dealt with accurately, requires a three-dimensional model. It has already been noted in section 2.2 that the nondimensional attenuation coefficient  $\alpha$  is insensitive to the separation of the rows in the array. Therefore, we choose to calculate a concentration,  $c$  say, in our arrays based on a cell that contains a single floe, and we write

$$c = \frac{A}{p^2}, \quad (4)$$

where  $A$  is the area of the fluid surface occupied by the floe and  $p$  is the periodicity length of the array.

[53] The value of  $c$  can be influenced in two ways: through the size of the floes and via the in-row spacing used. In Figure 10, we examine the way in which in-row separation affects attenuation. The floes that form the arrays here are circular, with 25 m radius, 0.5 m thickness, and include draft. As with previous cases, Figures 10a–10c are for periods of 8 s, 12 s, and 16 s, respectively.

[54] All three curves shown in Figure 10 demonstrate the intrinsic property of decreasing attenuation with increasing in-row separation. Over the 100 m interval used, the difference in attenuation is approximately an order of magnitude for all three periods, which implies that the behavior of the attenuation as a function of concentration is only weakly related to period. The curves display a slight, yet discernible, upward concavity, noting that  $\alpha$  is plotted on a logarithmic scale. The qualitative nature of the curves is similar in all cases except for a small interval around 40 m for the 8 s period. At this point, the kink in the curve can be attributed to the occurrence of a change in the number of waves supported by the array. This issue is an aspect of the periodicity that is required to facilitate our solution methods and, although only producing small anomalies such as the one shown here, as mentioned previously, it is something that will provide stimulus for the future development of our model.

[55] The results presented in Figure 10 are also presented in Figure 11, but with attenuation as a function of concentration,  $c$ , given in equation (4), rather than in-row separation. The data sets in this case are also overlaid with least squares straight-line fits, which demonstrate the linear dependence of attenuation on concentration, and we note the linear scale used for  $\alpha$  in these plots. This linear relationship is interrupted only over the interval in which the number of supported waves changes in the 8 s case, and, in this instance, two linear regimes are identified with similar gradients.

[56] From Figure 10, we may thus deduce that

$$\alpha \approx \alpha_0 + \alpha_1 c,$$

where the quantities  $\alpha_j$  ( $j = 0, 1$ ) are dependent on the properties of the floe and the incident wave only. It follows that the scaling of the attenuation is inversely proportional to the square of the in-row separation.

[57] Concentration can also be varied through the area of the fluid surface occupied by each floe. As we have already demonstrated a linear dependence of the attenuation on concentration, we will isolate its dependence on variations to the size of the floes by keeping concentration fixed. In a two-dimensional setting, *Kohout and Meylan* [2008] found that beyond a certain period-dependent value, floe length does not affect the attenuation in the model. This feature is related to the ability of a wave to induce the elastic response of a floe only when the ratio of the floe length to the ice-coupled wavelength is sufficiently large. Once this limit is obtained, any further increment to the floe length will be irrelevant, as waves are assumed to propagate without energy loss through regions of uniform ice cover. Conversely, relatively small floes act like rigid bodies. It is not immediately apparent that the simple behavior shown in the two-dimensional model will be replicated in three dimensions, where motions are not restricted to a single plane.

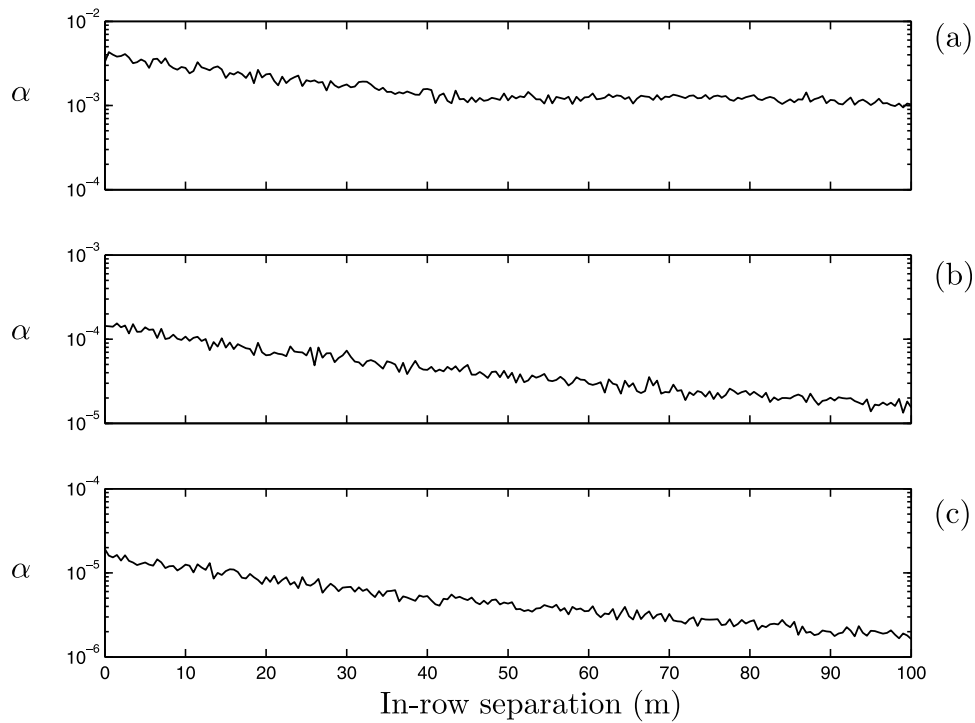


**Figure 10.** The attenuation coefficient as a function of in-row separation for period (a) 8 s, (b) 12 s, and (c) 16 s. The floes have radius 25 m and thickness 0.5 m.

[58] In Figure 12, the dependence of the attenuation on the horizontal extent of the floes that make up the array is explored. The floes used are circular, and we therefore show  $\alpha$  as a function of their radius and set the in-row separation to

be 20% of this to maintain a constant concentration. The periods 8 s, 12 s, and 16 s are shown, and in all cases the thicknesses of the floes are varied normally around the mean value of 1 m to eliminate length resonance.

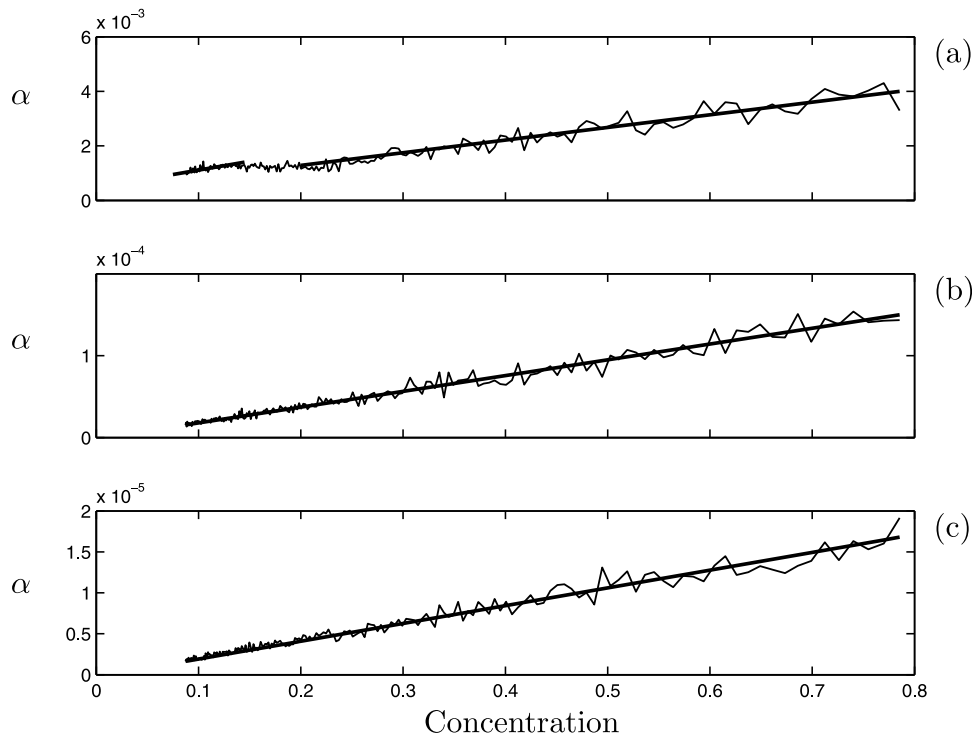


**Figure 11.** The attenuation shown in Figure 10, but as a function of concentration,  $c$ , given in equation (4). Straight-line fits are also shown (by thick lines).

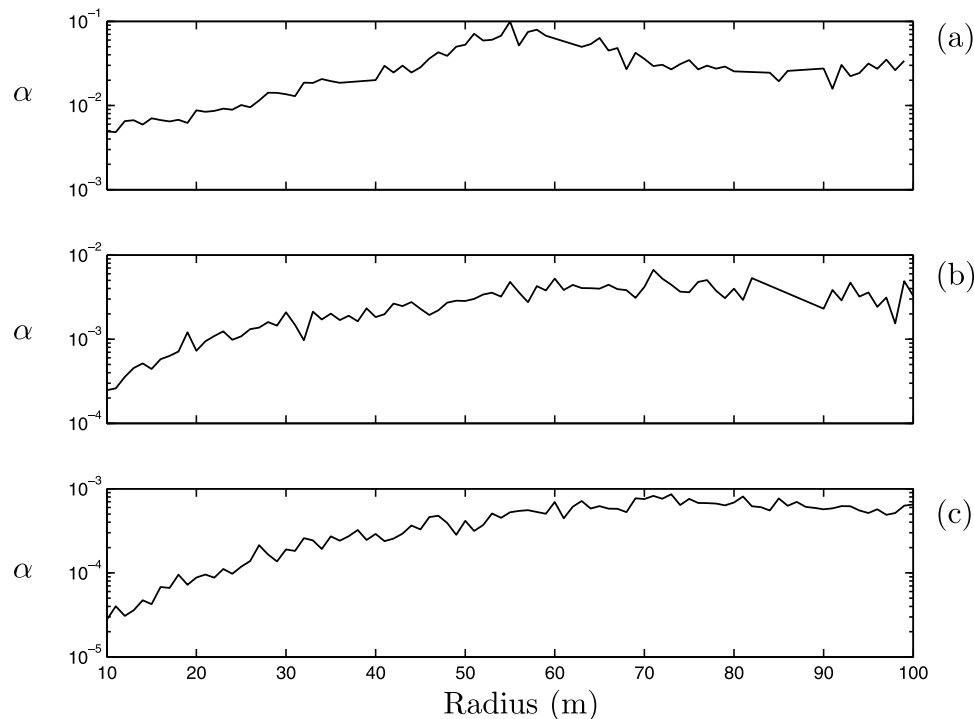


**Figure 12.** The attenuation coefficient as a function of floe radius for period (a) 8 s, (b) 12 s, and (c) 16 s. The floes have mean thickness 1 m and the in-row separation is 20% of the radius so that a constant concentration is maintained.

[59] As would be expected for the three chosen periods, we see that for relatively small floes, attenuation becomes greater as radius increases. This relationship becomes less important as the floes get larger until, at a radius of approximately 50–70 m, the attenuation is no longer affected by floe size variations. Our three-dimensional model therefore mirrors the behavior of a two-dimensional model in this respect. There is also evidence here that the size of the floes required to attain a stable attenuation coefficient increases as period increases, which concurs with our explanation of this property being governed by a relationship between floe length and wavelength. However, for 8 s, 12 s, and 16 s incident waves and a 1 m ice thickness, the ice-coupled wavelengths are 125 m, 226 m, and 394 m, respectively, and it is clear that the limit is not given by a simple ratio.

### 3.5. Comparison of the Three-Dimensional and Two-Dimensional Models

[60] Having made the above investigations into the dependence of the attenuation coefficient on the key parameters of the model, we now wish to compare the attenuation rates predicted by our new three-dimensional model with the existing two-dimensional model of *Kohout and Meylan* [2008]. In *Kohout and Meylan* [2008], the attenuation coefficient is plotted against period for a number of mean thicknesses, as these were found to be its two principal determinants when the floes are sufficiently long. From these data, the three sets with thicknesses 0.5 m, 1 m, and 2.5 m have been selected for comparison, and these are displayed in Figure 13.

[61] These results are shown alongside attenuation coefficients for our three-dimensional arrays with corresponding ice thicknesses. For consistency, and following from our investigation of the dependence of attenuation on floe size in the previous section, we use floes that are large enough that the attenuation coefficient has become insensitive to any further extension. We note that as the flexural rigidity of ice is strongly associated with its thickness, the size of the floes required to ensure a settled attenuation coefficient grows as their thickness increases. The concentration of the arrays is set as  $c = 0.5$ , although, as it results in only linear variations, this parameter is of little consequence on the logarithmic scale used here. As usual, the floes used in the arrays are circular and Archimedean draft is included.

[62] It is clear from Figure 13 that the models match reasonably well in a quantitative sense, with the corresponding attenuation coefficients never differing by more than an order of magnitude. As the two-dimensional model assumes homogeneity in one spatial dimension and therefore does not account for any open water between floes in this direction, it could be anticipated that it would cause more attenuation than the three-dimensional model. However, this comparison shows that the relationship between the two models is far more complicated, with the two-dimensional model producing greater attenuation for low periods and the three-dimensional model likewise for high periods. This is an interesting finding, as a consistent overprediction of attenuation for low periods and underprediction of attenuation for high periods has been observed when using two-dimensional models. We also note that the point at which these regimes interchange occurs at a higher period as thickness increases.

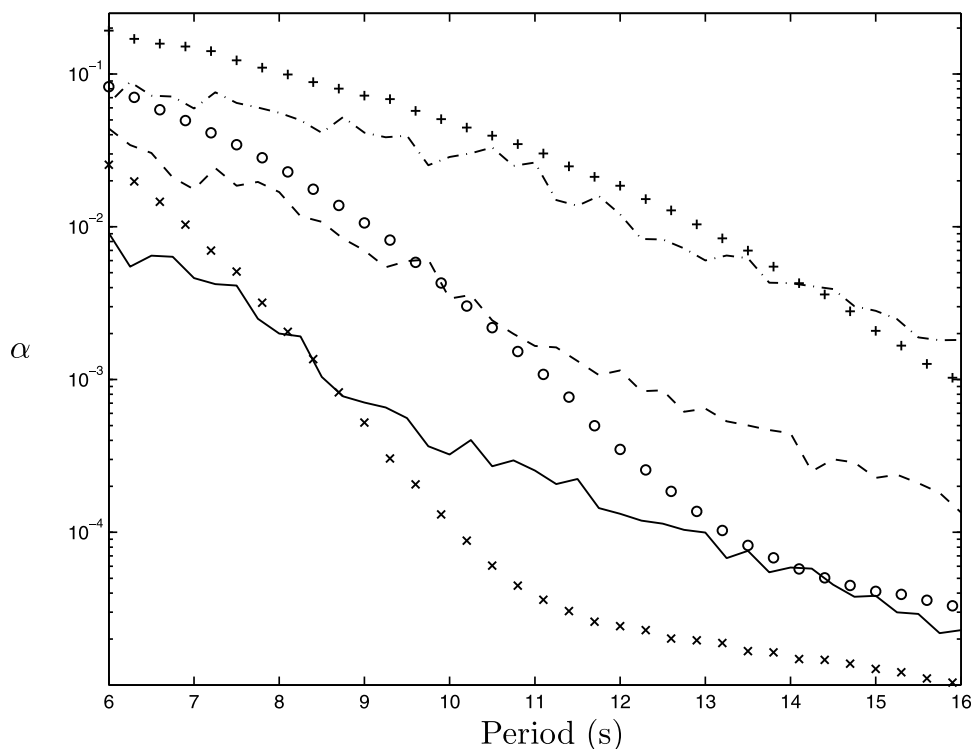


**Figure 13.** A comparison of the attenuation predicted by our three-dimensional model (lines) with that of the two-dimensional model of *Kohout and Meylan* [2008] (symbols) for large floes. Results for the three thicknesses  $D = 0.5$  m (solid lines and crosses), 1 m (dashed lines and circles), and 2.5 m (dot-dash lines and pluses) are given.

[63] Qualitatively, although the shape of the curves in the 2.5 m ice thickness case are alike, for the two thinner thicknesses, the attenuations predicted by the two models display distinct differences from one another. Whereas the attenuation coefficients of the two-dimensional model have prominent variations in curvature, on this logarithmic scale our attenuation coefficients are far straighter. The former may be a product of the transition between mass and flexure dominating the scattering process [*Vaughan et al.*, 2007], which is likely to be present for the 2.5 m thickness also but occurring for periods out of the chosen range. However, this feature is not present in the three-dimensional model where the ice cover consists of an infinite number of individual floes. The attenuation curves predicted by the three-dimensional model thus resemble those recently calculated by *Squire et al.* [2009] for attenuation in long transects sampled from submarine voyages in the Arctic Basin. We note, though, that the curves given here are generally not linear and display a slight concavity, which changes from upward for the thinner floes to downward for the thicker floes.

#### 4. Comparisons with Experimental Data

[64] Unfortunately, within the field of sea ice research, there are very few high-quality data sets that include measurements relating to the evolution of waves in the MIZ and are supported by robust contextual observations such as the physical properties of the sea ice and meteorological and oceanographic data. Indeed, at the time of this writing, the best available data were recorded 30 years ago. So, with the

adaptations the polar seas are currently experiencing due to climate change and the need to improve coupled models by properly assimilating the effects of wave-ice interactions, it is imperative that fresh efforts be made to perform experiments that will complement theoretical advances of the kind we have undertaken to create a synergy that progresses our understanding of this complicated phenomenon. In this context, a voyage has been scheduled for spring 2011 by the Australian Antarctic Division, which will, among other things, carry a group of researchers whose primary goal is to extract measurements of wave attenuation in ice-covered waters.

[65] Notwithstanding the dearth of suitable data and despite the limitations of the accompanying descriptions of the ice cover, it is still possible to gain some confidence about the performance of our model by comparing its predictions with the historical data referred to above, notably *Squire and Moore* [1980] and *Wadhams et al.* [1988].

##### 4.1. Bering Sea

[66] The MIZ wave attenuation experiment performed during a research cruise by NOAA Ship Surveyor in the Bering Sea during March 1979 [*Squire and Moore*, 1980] is, in all likelihood, the most complete single experiment of its kind done to date. While a wave buoy recorded off the ice edge, measurements were made at eight stations aligned with the principal swell and stretching almost 70 km into the ice pack. These data were processed to extract attenuation coefficients for five central wave periods. During the helicopter flights to and from the recording sites within the pack ice, ice

**Table 1.** Comparison of the (Dimensional) Attenuation Coefficients  $a$  Calculated During an Expedition in the Bering Sea in 1979 [Squire and Moore, 1980] Against Those Found From a Weighted Average of Results Given by the Three-Dimensional Model

Period (s)	Experimental $a \times 10^{-4}$ ( $\text{m}^{-1}$ )	Model $a \times 10^{-4}$ ( $\text{m}^{-1}$ )
12.2	$0.272 \pm 0.054$	0.030
9.4	$0.438 \pm 0.036$	0.201
7.6	$0.855 \pm 0.049$	0.813
6.4	$1.087 \pm 0.037$	1.567
5.5	$1.214 \pm 0.192$	3.237

concentration was estimated to be approximately 50%, and a zonal morphology, edge, transition, and interior delineating the approximate diameter of the floes was noted.

[67] The attenuation coefficient that is usually calculated in practice,  $a$ , say, is dimensional and such that

$$E \propto e^{-aL}$$

where  $L$  is the distance (in meters) into the ice pack. Consequently, to make a comparison with experimental data, we must first scale our nondimensional attenuation coefficient  $\alpha$  so that it describes attenuation per meter. To do this, we use the definition of the ice concentration  $c$  given in equation (4) and set

$$a = \alpha \sqrt{\frac{c}{A}},$$

recalling that  $A$  is the area of the fluid surface occupied by a single floe.

[68] Table 1 compares the experimental attenuation coefficients with attenuation coefficients calculated using the model reported herein. In keeping with the report of the ice conditions given by Squire and Moore [1980], we use  $c = 0.5$  as the ice concentration in our model and set the average thickness as  $D = 0.5$  m. To replicate the structure of the ice cover, three model runs were made in which the diameters of floes were 10 m, 25 m, and 100 m, these being the mean values across each zone, and the value of the attenuation determined for each zone was then used in a weighted average according to the proportion of the ice pack occupied by the relevant band.

[69] Given that the authors have had to idealize the formidable complexity and heterogeneity of a real MIZ and to interpret average parameters to describe the physical properties of the ice cover, the similarity between the experimental and model attenuation coefficients is most pleasing. In particular, we note that for all but the highest period, the attenuation coefficients are of the right order of magnitude. Better still is the agreement to the first significant figure for the 7.6 s and 6.4 s periods.

[70] As mentioned previously, the underprediction of attenuation for long waves in models that only accommodate scattering is well known. Such behavior should not be surprising, though, as the role of scattering is subordinate to dissipative processes in this regime [see Vaughan et al., 2009]. For this reason, the addition of viscosity to parameterize energy dissipation in the model, arising in both the water and, because of inelasticity, in the sea ice, is expected to

improve its accuracy, but this will be the topic of a future work. The overprediction of attenuation for short waves has also been observed previously, although it is less well understood. It may be due to unmodeled effects such as the nonlinear transfer of energy between frequencies, wave generation within the ice, or resonances, caused by wave-ice coupling, which create new waves that are not fully captured by the model. For the first time, the authors believe that the sophistication of the reported model will allow these more esoteric effects to be fully investigated, now that a robust and accurate three-dimensional characterization of MIZ scattering is in hand. Despite the presence of these foci for future model development, we are encouraged by the concurrence of theory and field experiment in the band of relevant periods, remembering that the model is parsimonious to the extent of any propitious parameterizations.

[71] In Squire and Moore [1980], a curve is given that shows how the diameter of an archetypal floe at a given penetration into the ice pack increases from 10 m at the ice edge to just over 100 m at 70 km. Using this distribution in our model, in Figure 14 we have produced the attenuation coefficient as a function of penetration for three wave periods. It is interesting to observe the differing behaviors of attenuation at the three periods considered. Only in the 7.6 s period case does the attenuation clearly display the sharp jump at around 35 km into the ice pack where the floe radius rapidly increases. In comparison, attenuation for a 12.2 s wave grows steadily to begin with, before beginning to level off, and for a 5.5 s wave, the attenuation appears to be insensitive to distance from the ice margin.

## 4.2. Kong Oscars Fjord

[72] During September 1979, the attenuation of wave energy was also measured in a fjord abutting the Greenland Sea. Conditions were more challenging there than in the Bering Sea, mainly because all the experiments had to be done from a land base at Mestersvig, a military outpost with a 1,800 m gravel runway located in Scoresby Land on the southern shore of Kong Oscars Fjord in Northeast Greenland National Park. This limited the measurements to within the fjord, which is not an ideal setting for monitoring the interaction of ocean waves with sea ice as factors such as reflections from the walls of the fjord, refraction, and a limited range of incidence angles (advantageous in some cases) influence experimental design. Despite these setbacks, full sets of data from two separate experiments were made, and the results were published by Wadhams et al. [1988] along with an account of the prevailing ice conditions described by Overgaard et al. [1983]. While suffering from the complications noted above, these data are regarded as a reliable addition to the Bering Sea measurements for comparison with the model.

[73] Of the two experiments that took place on 4 and 10 September, respectively, we select the former here as it is accompanied by a more comprehensive description of the prevailing ice conditions. The ice concentration was estimated at 0.3 and the diameters of the floes were in the range of 50 to 80 m. It was not possible to estimate a mean ice thickness, and we follow Kohout and Meylan [2008] in using the value given in the same location the previous year, which was 3.1 m. These ice properties are significantly different

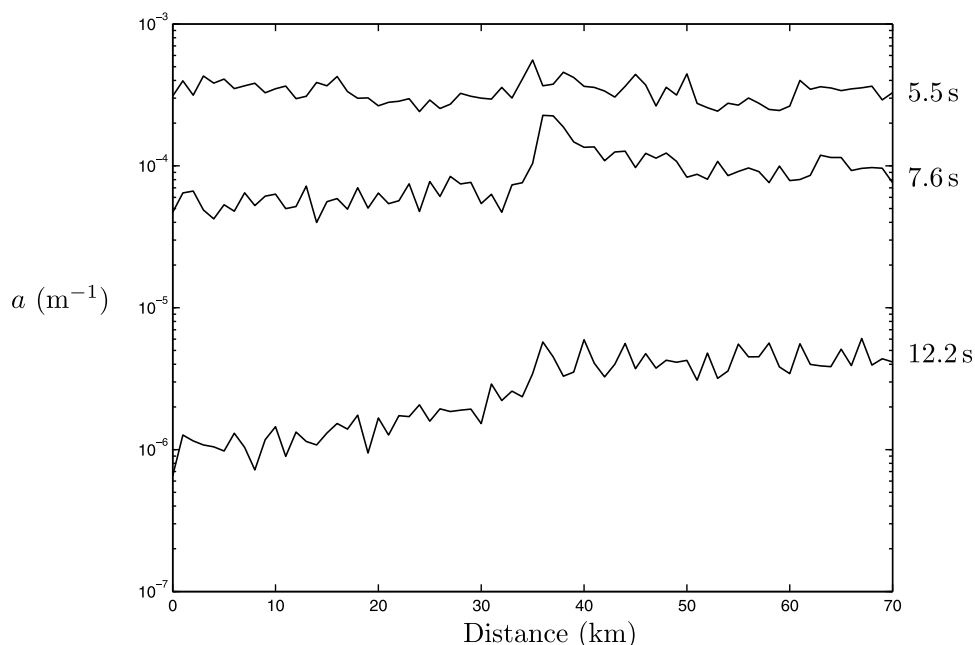


**Figure 14.** The (dimensional) attenuation coefficient  $a$  as a function of distance into the MIZ predicted by our model, where the properties of the ice pack are derived from data reported by *Squire and Moore* [1980].

from those in which the Bering Sea experiment was conducted, so the experiment provides a valuable second test case.

[74] Table 2 compares the experimental attenuation coefficients from 4 September in Kong Oscars Fjord with attenuation coefficients calculated using our model, with geometrical parameters intended to replicate, as best we can, the conditions reported during the experiment. Specifically, the floe diameter was set as 65 m, the concentration at  $c = 0.3$ , and the ice thickness was given a Gaussian distribution around the mean value 3.1 m and standard deviation 0.5 m.

[75] Again, we note that there is a general agreement to at least the order of magnitude between the experiment and model. However, it is evident in this case that the model underpredicts the attenuation when compared to the experiment and, in the four highest periods, this underprediction is approximately a factor of 2.4–2.65, becoming closer to the experimental value as period decreases. It is important to note, though, that these errors may not be related to the accuracy of the model, but rather to deficiencies in the reported experimental conditions, as noted earlier, or to an insufficient description of the ice state. Despite these hindrances, the similarities between the experiment and the model are reassuring.

[76] The experimental and model attenuation coefficients are extremely well matched for the lowest period. In regard to our earlier investigation, it is clear that the rapid change in the attenuation coefficient between 9.1 s and 8.14 s can be attributed to the addition of extra traveling waves at a nearby period, and our previous comments concerning this phenomenon apply. It is important not to become injudicious about the similarity of the attenuation predicted here, however, and we note that this indicates once more that the model attenuation coefficient is more sensitive to wave period than experimental data would suggest. On the other hand, we must not dismiss the fact that we have another example of

good agreement between the model and experimental data over a key range of periods.

## 5. Summary

[77] In this work, we have used a model, constructed to represent the passage of ocean waves through the MIZ, to study the rate of wave attenuation with respect to the properties of the ice cover and the incident wavefield. A three-dimensional description was employed, which treats the MIZ as a vast collection of separate floating elastic floes whose motions are interrelated. The model is based on the assumption of linear motions, and wave attenuation is caused only by the scattering produced by the floes. Flexure of the ice cover is identified as the main component of the propagation of wave energy, and other nonlinear effects such as inelasticity, turbulence, and inter-floe collisions are neglected.

[78] During the numerical investigation, the following discoveries were made. First, it was demonstrated that the attenuation coefficient has a roughly exponential dependence on the angle at which the incident ocean wave affects the array of floes, with oblique waves diminishing fastest. This provided an indication of some slight collimation, although at lower periods a contrasting spreading of the directional

**Table 2.** Comparison of the (Dimensional) Attenuation Coefficients  $a$  Calculated During an Expedition in the Greenland Sea on 4 September 1979 [*Wadhams et al.*, 1988] Against Those Calculated From Our Three-Dimensional Model

Period (s)	Experimental $a \times 10^{-4}$ ( $\text{m}^{-1}$ )	Model $a \times 10^{-4}$ ( $\text{m}^{-1}$ )
14.03	$0.29 \pm 0.27$	0.11
11.88	$0.73 \pm 0.25$	0.30
10.31	$1.23 \pm 0.19$	0.53
9.10	$2.01 \pm 0.17$	0.84
8.14	$2.66 \pm 0.22$	2.24

wavefield was evident. Next, it was shown that the addition of an Archimedean draft has an insubstantial effect on attenuation. Similarly, changing the shape and distribution of the floes was found to have little bearing on the attenuation produced by a large array. The attenuation predicted by the model was established as being directly proportional to the concentration of the ice cover. Furthermore, we studied how attenuation behaves in relation to the two determinants of concentration: floe spacing and floe diameter. It was noted that there is a limit at which attenuation becomes insensitive to the latter, but that for meaningful dimensions its value can differ by an order of magnitude according to the floe size present.

[79] Comparisons were also made of the three-dimensional model to an existing two-dimensional model and to two sets of experimental data of wave attenuation in the MIZ. For the former, it was clear that the three-dimensional model, in accordance with the two-dimensional model, is highly dependent on the average value of ice thickness and on wave period. Although, in the examples shown, the attenuation coefficients predicted by the two models did not differ by more than an order of magnitude, their qualitative appearance was distinct. In particular, the attenuation coefficients produced by the three-dimensional model were greater than the two-dimensional model for low periods and were smaller for high periods. Both comparisons with experimental data gave positive agreement and provided confidence in the model's ability to describe attenuation due to scattering. However, the familiar elements of underprediction for high periods and overprediction for low periods were still present.

[80] As mentioned in the introduction, we believe that the model providing the basis for this work contains the potential to be assimilated into an oceanic general circulation model. Therein our model would interact with embedded ice rheology and thermodynamic codes to provide information and predictions about the distribution of ocean wave activity in the sea ice and associated effects, such as wave-induced strain. The latter contribute to the morphological evolution of the ice pack along with deformations arising because of currents and winds acting through the large-scale sea-ice constitutive equation, e.g., viscous-plastic rheology. However, despite the encouraging performance that the model has shown in this work over meaningful ranges of periods, it is clear that opportunities still exist for its improvement. For instance, in terms of the interaction theory, we wish to eliminate the periodicity restraint, so that the rapid change in the attenuation coefficient over the intervals where additional waves cut in will be eliminated. Furthermore, methods must be developed to incorporate some nonscattering mechanisms, such as dissipation, into the model that will improve its accuracy in the high- and low-period regimes.

[81] As a final note, we reiterate that there is the promise of new data to complement our theoretical research in the near future. This is an exciting prospect and will certainly encourage further research to help replicate the physical situation as accurately as possible.

[82] **Acknowledgments.** This work was supported by the Marsden Fund Council from Government funding administered by the Royal Society of New Zealand. The authors also thank Alison Kohout for providing data for comparison.

## References

- Bennetts, L. G., and V. A. Squire (2009a), Linear wave forcing of an array of axisymmetric ice floes, *IMA J. Appl. Math.*, doi:10.1093/imamat/hpx038.
- Bennetts, L. G., and V. A. Squire (2009b), Wave scattering by multiple rows of circular ice floes, *J. Fluid Mech.*, 639, doi:10.1017/S0022112009991017.
- Bennetts, L. G., N. R. T. Biggs, and D. Porter (2007), A multi-mode approximation to wave scattering by ice sheets of varying thickness, *J. Fluid Mech.*, 579, 413–443.
- Bennetts, L. G., N. R. T. Biggs, and D. Porter (2009), Wave scattering by an axisymmetric ice floe of varying thickness, *IMA J. Appl. Math.*, 74, 273–295.
- Berry, M. V., and S. Klein (1997), Transparent mirrors: Rays, waves and localization, *Eur. J. Phys.*, 18, 222–228.
- Cathles, L. M., E. A. Okal, and D. R. MacAyeal (2009), Seismic observations of sea swell on the floating Ross Ice Shelf, Antarctica, *J. Geophys. Res.*, 114, F02015, doi:10.1029/2007JF000934.
- Dixon, T. W., and V. A. Squire (2001), Energy transport in the marginal ice zone, *J. Geophys. Res.*, 106, 19,917–19,927, doi:10.1029/2000JC000673.
- Feltham, D. L. (2008), Sea ice rheology, *Annu. Rev. Fluid Mech.*, 40, doi:10.1146/annurev.fluid.40.111406.102151.
- Hall, A. (2004), The role of surface albedo feedback in climate, *J. Clim.*, 17, 1550–1568.
- Kohout, A. L., and M. H. Meylan (2008), An elastic plate model for wave attenuation and ice floe breaking in the marginal ice zone, *J. Geophys. Res.*, 113, C09016, doi:10.1029/2007JC004434.
- Langhorne, P. J., V. A. Squire, and T. G. Haskell (2001), Lifetime estimation for a fast ice sheet subjected to ocean swell, *Ann. Glaciol.*, 33, 333–338.
- Linton, C. M., and P. McIver (2001), *Mathematical Techniques for Wave/Structure Interactions*, Chapman & Hall/CRC, Boca Raton, Fla.
- Linton, C. M., and I. Thompson (2007), Resonant effects in scattering by periodic arrays, *Wave Motion*, 44(3), 165–175.
- Masson, D., and P. LeBlond (1989), Spectral evolution of wind-generated surface gravity waves in a dispersed ice field, *J. Fluid Mech.*, 202, 111–136.
- McPhedran, R. C., L. C. Botten, A. A. Asatryan, N. A. Nicorovici, C. M. de Sterke, and P. A. Robinson (1999), Ordered and disordered photonic band gap materials, *Aust. J. Phys.*, 52, 791–809.
- Meylan, M. H. (2002), Wave response of an ice floe of arbitrary geometry, *J. Geophys. Res.*, 107(C1), 3005, doi:10.1029/2000JC000713.
- Meylan, M. H., and D. Masson (2006), A linear Boltzmann equation to model wave scattering in the marginal ice zone, *Ocean Model.*, 11, 417–427.
- Meylan, M. H., V. A. Squire, and C. Fox (1997), Towards realism in modeling ocean wave behavior in marginal ice zones, *J. Geophys. Res.*, 102(C10), 22,981–22,991, doi:10.1029/97JC01453.
- Overgaard, S., P. Wadhams, and M. Lepparanta (1983), Ice properties in the Greenland and Barents seas during summer, *J. Glaciol.*, 29(101), 142–164.
- Perrie, W., and Y. Hue (1996), Air-ice-ocean momentum exchange. Part 1: Energy transfer between waves and ice floes, *J. Phys. Oceanogr.*, 26, 1705–1720.
- Peter, M. A., and M. H. Meylan (2004), Infinite depth interaction theory for arbitrary floating bodies applied to wave forcing of ice floes, *J. Fluid Mech.*, 500, 145–167.
- Peter, M. A., and M. H. Meylan (2009a), Water-wave scattering by vast field of bodies, *SIAM J. Appl. Math.*, 70(5), 1567–1586.
- Peter, M. A., and M. H. Meylan (2009b), Water-wave scattering of vast fields of bodies such as ice floes in the marginal ice zone, in *Proc. 24th Int. Workshop on Water Waves and Floating Bodies, Zelenogorsk, Russia*, edited by A. Korobkin and P. Plotnikov.
- Peter, M. A., M. H. Meylan, and C. M. Linton (2006), Water-wave scattering by a periodic array of arbitrary bodies, *J. Fluid Mech.*, 548, 237–256.
- Porter, D., and R. Porter (2004), Approximations to wave scattering by an ice sheet of variable thickness over undulating bed topography, *J. Fluid Mech.*, 509, 145–179.
- Squire, V. A. (2007), Of ocean waves and sea-ice revisited, *Cold Reg. Sci. Technol.*, 49, 110–133.
- Squire, V. A., and S. C. Moore (1980), Direct measurement of the attenuation of ocean waves by pack ice, *Nature*, 283, 365–368.
- Squire, V. A., W. H. Robinson, M. H. Meylan, and T. G. Haskell (1994), Observations of flexural waves on the Erebus-Ice-Tongue, McMurdo-Sound, Antarctica, and nearby sea-ice, *J. Glaciol.*, 40(135), 377–385.
- Squire, V. A., J. P. Dugan, P. Wadhams, P. J. Rottier, and A. K. Liu (1995), Of ocean waves and sea ice, *Annu. Rev. Fluid Mech.*, 27, 115–168.

- Squire, V. A., G. L. Vaughan, and L. G. Bennetts (2009), Ocean surface wave evolution in the Arctic Basin, *Geophys. Res. Lett.*, *36*, L22502, doi:10.1029/2009GL040676.
- Timoshenko, S., and S. Woinowsky-Krieger (1959), *Theory of Plates and Shells*, 2nd ed., McGraw-Hill, New York.
- Vaughan, G. L., T. D. Williams, and V. A. Squire (2007), Perfect transmission and asymptotic solutions for reflection of ice-coupled waves by inhomogeneities, *Wave Motion*, *44*, 371–384.
- Vaughan, G. L., L. G. Bennetts, and V. A. Squire (2009), The decay of flexural-gravity waves in long sea-ice transects, *Proc. R. Soc. Lond. A*, *465*, 2785–2812.
- Wadhams, P. (1975), Airborne laser profiling of swell in an open ice field, *J. Geophys. Res.*, *80*, 4520–4528, doi:10.1029/JC080i033p04520.
- Wadhams, P. (1978), Wave decay in the marginal ice zone measured from a submarine, *Deep-Sea Res.*, *25*, 23–40.
- Wadhams, P. (1986), *The Geophysics of Sea Ice*, pp. 825–991, Plenum, New York.
- Wadhams, P., A. E. Gill, and P. F. Linden (1979), Transects by submarine of the East Greenland Polar Front, *Deep Sea Res.*, *26(A)*, 1311–1327.
- Wadhams, P., V. A. Squire, J. A. Ewing, and R. W. Pascal (1986), The effect of the marginal ice zone on the directional wave spectrum of the ocean, *J. Phys. Oceanogr.*, *16(2)*, 358–375.
- Wadhams, P., V. A. Squire, D. J. Goodman, A. M. Cowan, and S. C. Moore (1988), The attenuation rates of ocean waves in the marginal ice zone, *J. Geophys. Res.*, *93(C6)*, 6799–6818, doi:10.1029/JC093iC06p06799.
- Williams, T. D., and R. Porter (2009), The effect of submergence on the scattering by the interface between two floating plates, *J. Fluids. Struct.*, *25(5)*, 777–793.
- Williams, T. D., and V. A. Squire (2008), The effect of submergence on scattering across a transition between to floating flexible plates, *Wave Motion*, *45(3)*, 361–379.

---

L. G. Bennetts and V. A. Squire, Department of Mathematics and Statistics, University of Otago, PO Box 56, Dunedin, Otago 9054, New Zealand. (lbennetts@maths.otago.ac.nz)

M. H. Meylan, Department of Mathematics, University of Auckland, 38 Princes St., Auckland 1142, New Zealand.

M. A. Peter, Institute of Mathematics, University of Augsburg, 86135 Augsburg, Germany.